Journal of Catalysis 287 (2012) 55–61

Contents lists available at SciVerse ScienceDirect

Journal of Catalysis

journal homepage: www.elsevier.com/locate/jcat

Dynamics of direct H_2O_2 synthesis from H_2 and O_2 on a Pd nano-particle catalyst protected with polyvinylpyrrolidone

Takashi Deguchi, Hitoshi Yamano, Masakazu Iwamoto *

Chemical Resources Laboratory, Tokyo Institute of Technology, 4259-R1-5 Nagatsuta, Midori-ku, Yokohama 226-8503, Japan

ARTICLE INFO

Article history:
Received 28 October 2011
Revised 29 November 2011
Accepted 1 December 2011
Available online 2 January 2012

Keywords:
Hydrogen peroxide
Direct synthesis
Palladium catalyst
Pd–polyvinylpyrrolidone nano-particle
Reaction mechanism
Kinetics
Langmuir–Hinshelwood mechanism
Bromide adsorption
Reaction intermediate
Coordinative unsaturation

ABSTRACT

The kinetics of the H_2–O_2 reaction was studied on Pd–PVP (polyvinylpyrrolidone) nano-particles in water. With H^+ and Br^-, Pd–PVP catalyzed the H_2O_2 synthesis. H_2 and O_2 partial pressure dependencies revealed that the H_2O_2 formation followed the Langmuir–Hinshelwood mechanism and that the H_2O_2 selectivity varied greatly with p_{H2}, which was quite different from the results using Pd/C. In the absence of Br^-, the H_2–O_2 reaction primarily yielded H_2O, and the reaction rate was very high and proportional to p_{H2}. Br^- adsorption measurements suggested that the proportion of highly unsaturated sites on Pd–PVP was much higher than on Pd/C. In the presence of H^+ and Br^-, the most unsaturated sites such as a corner site of the Pd particles would be blocked by the HBr adsorption and inert, and the major reaction would proceed on moderately unsaturated sites such as an edge site, which stabilize intermediates more than the least unsaturated sites such as a plane site.

1. Introduction

The catalytic synthesis of H_2O_2 from H_2 and O_2 in the liquid phase has been extensively studied due to industrial utilization of H_2O_2 and interest in the mechanism of the selective oxidation of H_2 [1–3]. Pd, Pt, Au and their alloys have been employed as catalysts with and without proton and halide ions, such as Cl^- or Br^-. In addition to the development of active catalysts, research has focused on the kinetics and reaction mechanism as well as the active phases and sites of the catalysts. It was widely accepted that the kinetic analysis was limited due to the complicated reaction routes illustrated in Scheme 1 and the difficult calculation of the mass transfer processes in the three-phase system. We recently reported the systematic measurement of the kinetics, including the mass transfer processes, for the Pd/C catalyst [4], which allowed for the determination of the reaction mechanism. For example, in the H_2–O_2 reaction on the Pd/C in the presence of H^+ and Br^- under p_{H2} of 0–18 kPa and p_{O2} of 0–90 kPa, the activation of H_2 was rate determining, whereas O_2 exhibited a Langmuir–Hinshelwood (L–H) type retarding effect. The proposed mechanism involved the hydrido-hydroperoxy species H–M–OOH (M, metal surface) as the key intermediate of H_2O_2 formation, direct H_2O formation, and H_2O_2 destruction [5]. In addition, two types of metal surface sites were proposed in which one exhibits a high degree of coordinative unsaturation that would catalyze both the direct H_2O formation and the H_2O_2 decomposition. The reactions would be inhibited by adsorption of the pairs of Br^- and H^+ ions. Another type of metal surface site is a flat surface with a low degree of unsaturation that would be active for H_2O_2 formation.

The locations of the active sites and their relative activity might be dependent on the supports. Application of the kinetic analysis method developed by our group [4,5] to Pd nano-colloid catalyst particles would be an efficient approach for the clarification of the active sites on Pd because the colloid particles would minimize the effect(s) of the supports. In fact, various Pd colloids have already been examined as catalysts in solution with or without supports [6,7], although the kinetics of the reactions was not necessarily studied. Pd colloid has also been proposed as the active phase in the H_2–O_2 reaction on the Pd/SiO_2 catalyst [8,9]. Herein, we performed kinetic studies using Pd nano-colloids protected by polyvinylpyrrolidone (Pd–PVP) and found a different kinetic behavior compared to the Pd/C catalyst. The difference in the kinetics is discussed from the viewpoint of the active sites on the Pd surface.

* Corresponding author.
E-mail address: iwamoto@res.titech.ac.jp (M. Iwamoto).

0021-9517/$ - see front matter © 2011 Elsevier Inc. All rights reserved.
doi:10.1016/j.jcat.2011.12.004

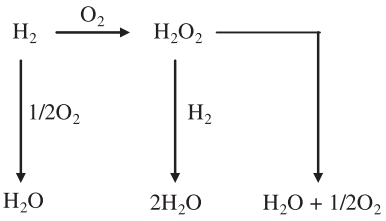

Scheme 1. Reactions involved in the direct H_2O_2 synthesis.

2. Experimental and data processing

2.1. H_2–O_2 reaction

The reaction apparatus was improved from the one used in our previous work [4]. The reaction was performed in a 300-ml flat bottom separable flask made of Pyrex glass with an inner diameter of 80 mm equipped with a magnetic stirrer, a gas feed nozzle, a liquid sampling nozzle, and a thermometer. A cross-shaped rotor with a length of 50 mm and a height of 15 mm was employed. To avoid ignition by static electricity, all apparatus parts were made of stainless steel tube with an inner diameter of 1 mm except for the reactor. The dead volume in the reactor was minimized, and a glass plug was placed in the reactor as a safety valve. The Pd–PVP colloid solution was provided by Tanaka Kikinzoku Kogyo K.K., Japan, and used for the catalytic experiments as received. The average particle size was determined from the transmission electron microscope (TEM) image (Fig. S1 in supplementary information) and was found to be approximately 3.6 nm. All of the gases used were of industrial grade, and the flow rates were controlled by mass flow controllers.

The colloid solution containing 2.5 mg of Pd (3 ml of the solution) was introduced into a prescribed amount of water in the flask and activated with H_2 at 30 °C for 40 min. Subsequently, N_2 gas was introduced to displace the H_2 gas, and the additive(s) was added in the form of an aqueous solution. H_2SO_4 and NaBr were employed as the H^+ and Br^- sources, respectively. Finally, the volume of the solution was adjusted to 300 ml. After sufficient displacement with N_2, the mixture of H_2, O_2, and N_2 gases was passed into the reactor through the nozzle, and the gas composition was analyzed by gas chromatography every 10 min using N_2 as the internal standard to determine the consumption of H_2 and O_2. The reaction temperature was maintained at 30 °C, and the agitation rate was 1200 rpm. It is important to note that the gas composition was often within the flammable range.

The data in the initial unsteady period resulting from the dead volume of the reactor were treated in the following way. When V_G and F_G represent the gas phase dead volume and the rate of gas flow out of the reactor, respectively, the corrected initiation time (t_0) was approximated by $t_0 = V_G/F_G$ (in general, t_0 was approximately 5 min). Because the measured gas composition became nearly stationary after an elapse time of 20 min, the corrected initial gas composition was determined by linear extrapolation of the analyzed compositions of the three successive samples collected after time $t = 20$ min to time $t = t_0$.

The rates of H_2O_2 and H_2O formation were calculated using Eqs. (1) and (2) where r_0 and r_{O2} are the rates of H_2 and O_2 consumption, respectively.

$$d[H_2O_2]/dt = 2r_{O2} - r_0 \quad (1)$$

$$d[H_2O]/dt = 2r_0 - 2r_{O2} \quad (2)$$

$[H_2O_2]$ was calculated by numerical integration of Eq. (1) at each sampling point. The actual $[H_2O_2]$ was analyzed at the final sampling time with a UV–Vis absorption method using a titanium sulfate solution, and it was found to be nearly equal to the calculated value as demonstrated in Fig. S2 in supplementary information.

For analysis of the reaction parameters, we used Eq. (3) [4] in which S_f and k_d represent the H_2O_2 formation selectivity and the H_2O_2 destruction rate constant, respectively, which include the p_{H2} and p_{O2} terms. Eq. (4) was derived by integration of Eq. (3) followed by the subsequent rearrangement of the resulting equation. Here, Σ_1 and Σ_2 are defined as $\Sigma_1 = \int r_0 dt$ and $\Sigma_2 = \int [H_2O_2] dt$, respectively.

$$d[H_2O_2]/dt = r_0 S_f - k_d[H_2O_2][Cat] \quad (3)$$

$$\Sigma_1/[H_2O_2] = 1/S_f + (k_d[Cat]/S_f)\Sigma_2/[H_2O_2] \quad (4)$$

The intercept and the slope of the correlation line of $\Sigma_1/[H_2O_2]$ and $\Sigma_2/[H_2O_2]$ yield $1/S_f$ and $k_d[Cat]/S_f$, respectively. In fact, the following approximations were applied for each time t_j ($j = 0, 1, 2, \ldots$).

$$(\Sigma_1)_j = \Sigma((r_0)_j + (r_0)_{j-1})(t_j - t_{j-1})/2 \quad (5)$$

$$(\Sigma_2)_j = \Sigma([H_2O_2]_j + [H_2O_2]_{j-1})(t_j - t_{j-1})/2 \quad (6)$$

2.2. Br-adsorption

The method described in the previous paper [5] was modified. The catalyst was activated using the procedure described above. N_2 was then introduced to displace H_2. The H_2SO_4 and NaBr solutions with the desired concentrations were added. The mixture was agitated at 30 °C for 1 h under N_2 atmosphere. Then, 5 ml of the solution was quickly transferred to an ultrafiltration device (Vivaspin 6, MW 50,000; Sartorius Stedim Biotech S.A.) and filtered (in 3 min). The Br^- concentration in the filtrate was measured using ion chromatography. It was confirmed by a separate experiment that the concentration of Br^- in the filtrate was nearly the same as the original aqueous solution containing Br^- and that Pd was not detected in the filtrate when the Pd–PVP solution was filtered.

3. Results and discussion

3.1. Effects of H_2 and O_2 partial pressures on H_2O_2 synthesis on Pd–PVP

3.1.1. Time course of the H_2O_2 synthesis

Prior to performing a detailed kinetic study, the performance and stability of the present catalytic system was confirmed. Fig. 1

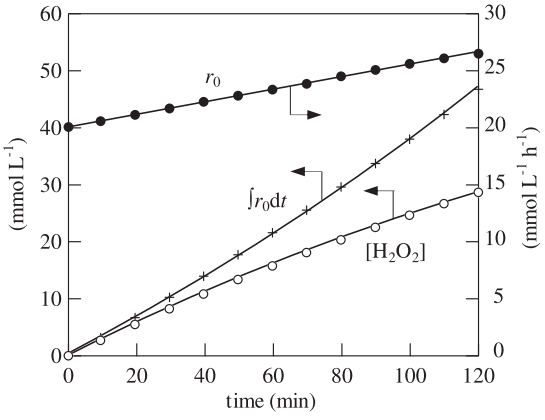

Fig. 1. Typical time course of the H_2–O_2 reaction catalyzed by Pd–PVP colloid catalyst: 8.33 mg L^{-1}, with 0.01 N H_2SO_4, 0.001 N NaBr, p_{H2} 16–17 kPa, p_{O2} 37 kPa, 30 °C, and 1200 rpm.

illustrates a typical example of the time course of the H_2–O_2 reaction on Pd–PVP in the presence of H^+ and Br^-. Unexpectedly, r_0 was found to increase gradually. However, a linear relationship between $\Sigma_1/[H_2O_2]$ and $\Sigma_2/[H_2O_2]$ was confirmed, as shown in Fig. S3.1 in supplementary information, demonstrating the validity of Eqs. (3) and (4) for this catalyst system. Because the H_2 reaction rate varied with the reaction time, we will hereafter discuss the rate in terms of the initial value of r_0. Fig. S3.2 in supplementary information shows the relationship between the increments in r_0 and $d[H_2O]/dt$ based on the values obtained at t_0. $\Delta(d[H_2O]/dt)$ was proportional to Δr_0, and the slope was found to be 2, indicating that the increment of r_0 resulted from the formation of water (Eq. (7)). This result will be discussed later.

$$H_2O_2 + H_2 \rightarrow 2H_2O \tag{7}$$

3.1.2. Dependence of the H_2O_2 synthesis on H_2 and O_2 partial pressures

Figs. 2 and 3 summarize the correlation of the H_2 and O_2 partial pressures with the catalysis on Pd–PVP in the presence of H^+ and Br^-. The H_2 consumption rate, r_0, increased with increasing p_{H2} and p_{O2} and then became approximately fixed in both cases. The value of S_f increased when p_{H2} increased, whereas S_f was only slightly dependent on p_{O2}. This is consistent with the results of Chinta and Lunsford who found that a larger O_2/H_2 ratio resulted in a smaller H_2O_2 selectivity on their catalyst system, which contained colloidal Pd [10]. The k_d value increased with p_{H2}; however, the rate of change was reduced at a higher p_{H2}, whereas k_d decreased with increasing p_{O2}. The H_2 concentration in the liquid phase, $[H_2]$, was calculated using Eq. (8), which was derived in a previous paper [4]. In Eq. (8), H and k_La are Henry's law constant for H_2 and the mass transfer coefficient of H_2. The value of k_La for the present reaction system was 1140 h^{-1} (Fig. S4.2 in supplementary information). In Fig. 2, the values of $[H_2]/[H_2]^*$ are plotted in which $[H_2]^*$ is the H_2 concentration equilibrated with p_{H2}. $[H_2]/[H_2]^*$ varied from approximately 0.5 to approximately 0.9.

$$[H_2] = p_{H2}/H - r_0/k_La \tag{8}$$

The dependence of r_0 on the H_2 and O_2 partial pressures was analyzed using a kinetic model based on the L–H mechanism. When

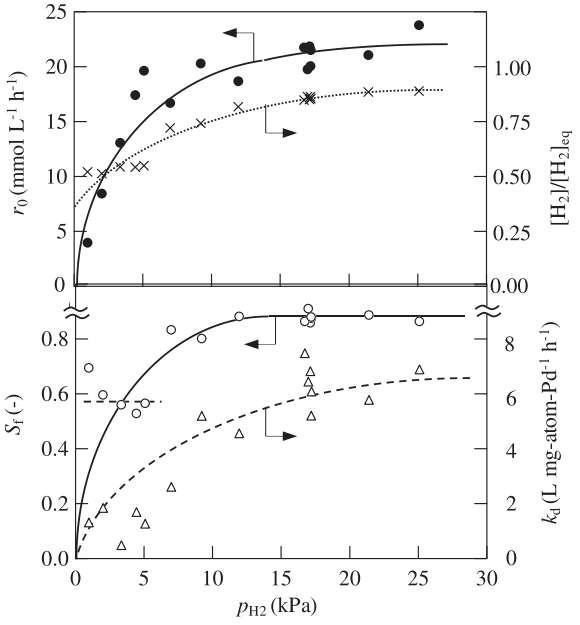

Fig. 2. Effects of the p_{H2} on the kinetic parameters of the H_2–O_2 reaction catalyzed by Pd–PVP colloid: 8.33 mg-Pd L^{-1} with 0.01 N H_2SO_4, 0.001 N NaBr, p_{O2} 35–37 kPa, 30 °C, and 1200 rpm.

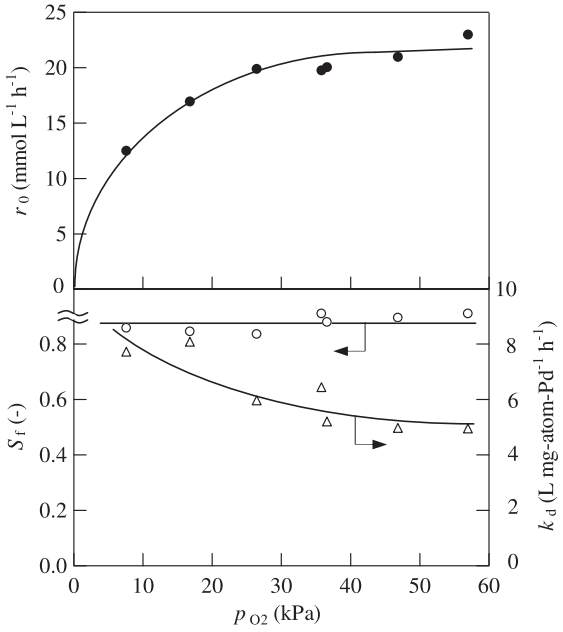

Fig. 3. Effects of the p_{O2} on the kinetic parameters of the H_2–O_2 reaction catalyzed by Pd–PVP colloid: 8.33 mg-Pd L^{-1} with 0.01 N H_2SO_4, 0.001 N NaBr, p_{H2} 17–19 kPa, 30 °C, and 1200 rpm.

most of the active sites are covered by adsorbed H and O_2 and the amounts of adsorbed H_2 and O_2 are in equilibrium (Eqs. (9) and (10)), the reaction between the adsorbed species or the subsequent reaction (Eq. (11)) is the rate-determining step, whose reaction rate can be expressed by Eq. (12). This equation can be changed to Eq. (13) using Eq. (10). In the equations, K_1 and k_1 are the equilibrium constant and the rate constant, respectively, and $[M]_0$ (=$[MH_2]$ + $[M(O_2)]$) represents the concentration of the active sites. Eq. (13) is transformed to Eq. (14) in which $k_{10} = k_1K_1[M]_0^2$, which suggests that a linear relationship exists between $([H_2]/[O_2]/r_0)^{1/2}$ and $[H_2]/[O_2]$.

$$M(O_2) + H2 \overset{K_1}{\rightleftarrows} MH_2 + O_2 \tag{9}$$

$$K_1 = [MH_2][O_2]/[M(O_2)]/[H_2] \tag{10}$$

$$MH_2 + M(O_2) \overset{k_1}{\rightarrow} \overset{(slow)}{\rightarrow} H_2O_2 \tag{11}$$

$$r_0 = k_1[MH_2][M(O_2)] \tag{12}$$

$$r_0 = k_1K_1[M]_0^2[H_2][O_2]/(K_1[H_2] + [O_2])^2 \tag{13}$$

$$([H_2]/[O_2]/r_0)^{1/2} = k_{10}^{-1/2}(1 + K_1[H_2]/[O_2]) \tag{14}$$

In fact, $([H_2]/[O_2]/r_0)^{1/2}$ and $[H_2]/[O_2]$ exhibited a linear relationship, as shown in Fig. 4, in which $[O_2]$ was replaced by $[O_2]^*$, the concentration of O_2 in water equilibrated with p_{O2}, because p_{O2} was much higher than p_{H2}, and therefore, the deviation of $[O_2]$ from $[O_2]^*$ would be very small during the reaction. It should be noted that the kinetic handling of the dissociatively adsorbed H_2 in Eqs. (10) and (12) lacked strictness. However, it was reasonably confirmed that the reaction proceeded via the L–H mechanism.

Voloshin et al. reported that the H_2–O_2 reaction on a 2%-Pd/SiO_2 catalyst in the presence of 0.2 N–H_2SO_4 and 0.0001 N–NaBr followed an L–H rate expression under p_{H2} up to approximately 200 kPa and p_{O2} up to approximately 400 kPa in a microreactor [11]. In contrast, the pressure ranges applicable for the L–H rate expression on the present catalyst were 0–15 and 0–30 kPa for

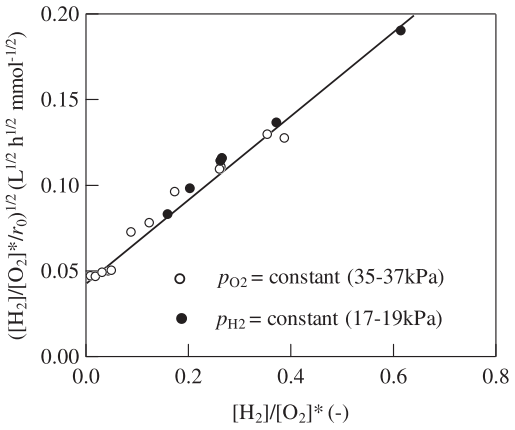

Fig. 4. $([H_2]/[O_2]^*/r_0)^{1/2}$ as a function of $[H_2]/[O_2]^*$ according to Eq. (12) and based on the data shown in Figs. 4 and 5.

P_{H2} and P_{O2}, respectively, which most likely indicates much higher stability of the adsorbed species. In addition, the non-linear dependence of r_0 on p_{H2} makes it difficult to determine the intrinsic activity of the Pd–PVP catalyst based on the mass transfer treatment introduced in the previous study [4]. Therefore, the kinetics is discussed here using r_0 without additional treatment.

3.1.3. Dependence of H_2O_2 hydrogenation on H_2 partial pressure

The p_{H2} dependence of the H_2O_2 hydrogenation on the Pd–PVP catalyst was similar to that observed for the H_2–O_2 reaction as shown in Fig. 5, being also consistent with an L–H mechanism. Replacement of O_2 with H_2O_2 and subscript 1 with 2 resulted in the derivation of Eqs. (15)–(20) from Eqs. (9)–(14). As shown in Fig. S5 in supplementary information, the plot of $[H_2]/[H_2O_2]$ as a function of $([H_2]/[H_2O_2]/r_0)^{1/2}$ exhibited a linear relationship, which supports the L–H mechanism.

$$M(H_2O_2) + H_2 \overset{K_2}{\rightleftarrows} MH_2 + H_2O_2 \tag{15}$$

$$K_2 = [MH_2][O_2]/[M(H_2O_2)]/[H_2] \tag{16}$$

$$MH_2 + M(H_2O_2) \overset{k_2}{\rightarrow} \overset{\text{(slow)}}{\rightarrow} 2H_2O \tag{17}$$

$$r_0 = k_2[MH_2][M(H_2O_2)] \tag{18}$$

$$r_0 = k_2K_2[M]_0^2[H_2][H_2O_2]/(K_2[H_2] + [H_2O_2])^2 \tag{19}$$

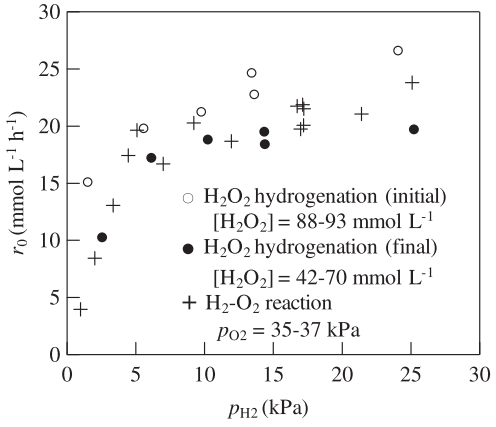

Fig. 5. Comparison of the dependence of the p_{H2} on the H_2O_2 hydrogenation and the H_2–O_2 reaction catalyzed by Pd–PVP colloid: 8.33 mg-Pd L^{-1} with 0.01 N H_2SO_4, 0.001 N NaBr, p_{H2} 17–19 kPa, 30 °C, and 1200 rpm.

$$([H_2]/[H_2O_2]/r_0)^{1/2} = k_{20}^{-1/2}(1 + K_2[H_2]/[H_2O_2]) \tag{20}$$

In the above experiments, the kinetics of the synthesis and hydrogenation of H_2O_2 was individually investigated. The kinetic expression for the consecutive reactions of Eqs. (9), (11), (15), and (17) could be expressed as shown in Eq. (21).

$$r_0 = \frac{(k_1/K_1)[M]_0^2[H_2][O_2] + (k_2/K_2)[M]_0^2[H_2][H_2O_2]}{([H_2] + [O_2]/K_1 + [H_2O_2]/K_2)^2} \tag{21}$$

When the $[H_2O_2]/K_2$ term is negligible compared to other terms in the denominator, r_0 would linearly increase with increasing $[H_2O_2]$ (i.e., the increment of r_0 should correspond to the H_2O_2 hydrogenation rate). The change in r_0 with the reaction time in Fig. 1 and the relationship between the increments of r_0 and H_2O formation rate in Fig. S3.2 in supplementary information were consistent with Eq. (21). Moreover, Eq. (21) was consistent with L–H type depression effect of O_2 on k_d, as shown in Fig. 3, assuming that the H_2O_2 destruction was primarily caused by hydrogenation.

3.2. Effects of H^+ and Br^- concentrations on the H_2–O_2 reaction on Pd–PVP

3.2.1. p_{H2} and p_{O2} dependencies of H_2–O_2 reaction in the absence of Br^-

Fig. 6 shows the p_{H2} and p_{O2} dependence of the H_2–O_2 reaction on Pd–PVP in the absence of Br^-. It is important to note that the catalyst concentration was 1/3 of that used to obtain the results shown in Fig. 2 to suppress the reaction rate. The reaction rate was much higher than in the presence of H^+ and Br^-, and water was the sole product. The rate was proportional to the p_{H2} and exhibited an L–H type depression effect for O_2 in the presence and absence of H_2SO_4. The observations suggested that the sites blocked by Br^- in the presence of Br^- otherwise exhibited a high ability to directly burn H_2. The rate in the presence of H_2SO_4 was higher than without H_2SO_4, which can be explained by the enhancement of the β-elimination of the key intermediate H–M–OOH by H^+, as described in a previous paper [5].

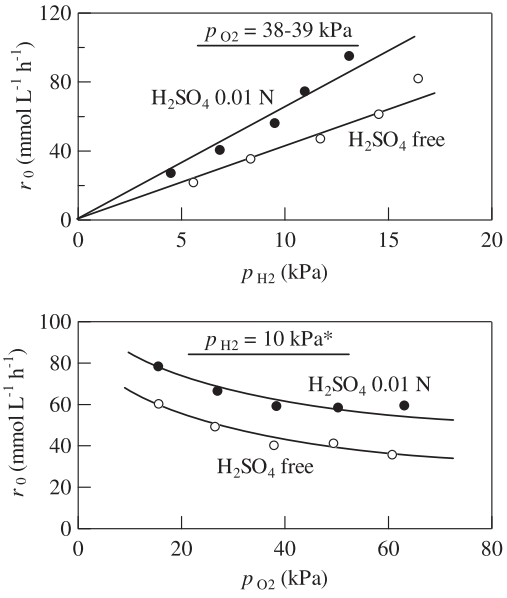

Fig. 6. Dependence of the p_{H2} and the p_{O2} for the H_2–O_2 reaction catalyzed by Pd–PVP colloid: 2.78 mg-Pd L^{-1} in the absence of Br^- at 30 °C, and 1200 rpm. *r_0 was reduced to the value for p_{H2} = 10 kPa by multiplying 10/(actual p_{H2}; 8–12 kPa).

In Fig. 6, the linear correlation between p_{H2} and r_0 permitted us to analyze the rate including the mass transfer process of H_2, which would allow for the determination of the intrinsic activity of the catalyst system. Eq. (22) [4] was applied where k_{0a} and k_0 are the apparent rate constant defined by Eq. (23) and the intrinsic rate constant, respectively.

$$1/k_{0a} = 1/k_0 + [\mathrm{Cat}]/(k_L a/\mathrm{H}) \quad (22)$$

$$r_0 = k_{0a} p_{H2} [\mathrm{Cat}] \quad (23)$$

The values of k_0 with and without H_2SO_4 were 900 and 320 mol g-atom-Pd^{-1} h^{-1} kPa^{-1}, respectively. The values on the 5%-Pd/C catalyst in the absence of Br$^-$ [5] were 105 and 59 mol g-atom-Pd^{-1} h^{-1} kPa^{-1}, respectively. Therefore, the intrinsic activities of Pd–PVP with and without H_2SO_4 were 8.6 and 5.4 times higher respectively than those of Pd/C. When the activity per the site inactivated in the presence of H$^+$ and Br$^-$ on the Pd–PVP was approximately equal to that on the Pd/C, the results suggest that the number of the inactivated sites was much larger on Pd–PVP than on Pd/C.

3.2.2. Influence of H$^+$ and Br$^-$ concentrations on the H_2O_2 synthesis

The effect of the concentration of H$^+$ added, $[H^+]_{added}$, under constant and high [Br$^-$] conditions (Series I) and the concentration of Br$^-$ added, $[Br^-]_{added}$, under constant and high [H$^+$] condition (Series II) was examined, and the results are summarized in Fig. 7. The r_0 value decreased with increasing $[H^+]_{added}$ and $[Br^-]_{added}$, indicating HBr adsorption on the active sites (Eq. (24)), which has been previously discussed [5].

$$\mathrm{M} + \mathrm{H}^+ + \mathrm{Br}^- \leftrightarrows \mathrm{H-M-Br} \quad (24)$$

It would be reasonable to assume that Pd–PVP contained HBr-adsorbable sites in larger quantities than Pd/C. In Series I, many of the active sites were blocked even at low H$^+$ concentrations while the Br$^-$ added efficiently blocked the active sites steeply depressing r_0 in Series II. The H_2O_2 selectivity (S_f) rose dramatically with $[Br^-]_{added}$ in Series II and was then nearly constant, as shown in Fig. 7b (solid line). These results indicated that the sites with low selectivity were blocked first and followed by those with higher selectivity. The S_f value also rose gradually with $[H^+]_{added}$ in Series I, which was mostly likely due to the first effect of H$^+$ aiding the HBr adsorption (Eq. (23)) followed by the second effect of H$^+$ accelerating the H_2O_2 desorption [5].

3.2.3. Br$^-$ adsorption on Pd–PVP

Measurement of the Br$^-$ adsorption equilibrium on Pd–PVP was performed according to the previously published protocol [5] with two modifications. First, ultrafiltration was applied to separate the Br$^-$ solution and the colloid catalyst as described in the Experimental section. Second, the sweeping treatment with O_2 [5] to eliminate hydride species produced upon H_2 reduction on the catalyst was omitted, because it was found that the amount of adsorbed Br$^-$ decreased by the O_2-sweeping to less than half of that on the Pd–PVP without the treatment. This might result from a change in the relative adsorbability of HBr, H_2, H_2O_2, and O_2 on Pd catalysts (e.g., H_2 > HBr > O_2 on Pd/C while O_2 > HBr > H_2 on Pd–PVP). Unfortunately, the change implied that the Br$^-$ adsorption measurement was not suitable for the quantitative characterization of the Pd surface, but the following measurements were performed as they were expected to provide useful information about the surface.

Fig. 8 shows the atomic ratios of the adsorbed Br$^-$ to the total amount of Pd ($[Br^-]_{ad}/[Pd]_0$) on Pd–PVP and Pd/C as a function of $[H^+]^{1/2}[Br^-]^{1/2}$. The data reported in our previous paper were also plotted for comparison. For the Pd–PVP, the $[Br^-]_{ad}/[Pd]_0$ ratio was nearly constant within the measurement range and high even at very low $[H^+]^{1/2}[Br^-]^{1/2}$, which was in good agreement with the observation that Pd–PVP has more HBr-adsorbable sites than Pd/C. It is important to note that the Pd/C catalyst exhibited very low $[Br^-]_{ad}/[Pd]_0$ values at 0–0.1 and 0.2–0.3 × 10^{-4} N of $[H^+]^{1/2}[Br^-]^{1/2}$ after treatment with O_2 and H_2, respectively. This is most likely due to the change in the order of the relative adsorbability of HBr, H_2, H_2O_2, and O_2, as described in the previous paragraph. The difference between the adsorbability of Br$^-$ on Pd–PVP and Pd/C should be clarified in the future. Fig. 8 also showed that the $[Br^-]_{ad}/[Pd]_0$ values for both catalysts were roughly the same at higher $[H^+]^{1/2}[Br^-]^{1/2}$, irrespective of the pretreatment, which indicated that the upper limit of $[Br^-]_{ad}/[Pd]_0$ was independent of the type of catalyst. However, under the H_2–O_2 reaction conditions, Br$^-$ would be exposed to heavy competition with H_2 and O_2 for the adsorption sites. Br$^-$ would adsorb more easily onto the coordinatively more unsaturated sites [5].

3.3. Discussion of the active sites on Pd catalysts

3.3.1. Classification of the observed kinetics

The kinetic behaviors of the Pd–PVP catalyst were distinctly different from those of the Pd/C catalyst [5]. On Pd–PVP, H_2O_2

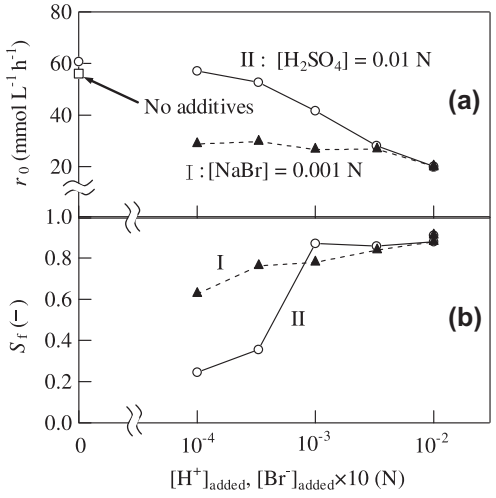

Fig. 7. Effects of H$^+$ and Br$^-$ concentrations on the H_2–O_2 reaction catalyzed by Pd–PVP colloid: 8.33 mg-Pd L^{-1} with a H_2 feed rate of 10 sccm (p_{H2} 8–17 kPa), an O_2 feed rate of 20 sccm (p_{O2} 35–37 kPa), and a N_2 feed rate of 20 sccm at 30 °C and 1200 rpm.

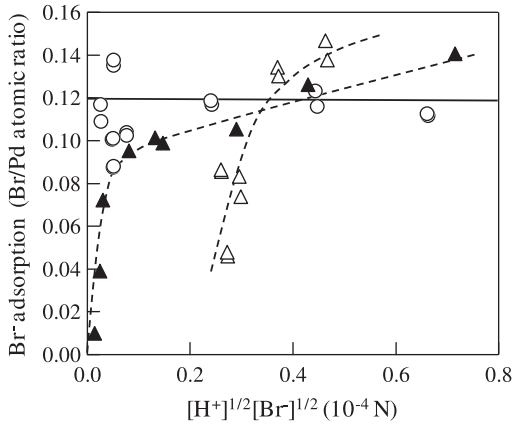

Fig. 8. Br-adsorption as a function of H$^+$ and Br$^-$ concentrations. ○ Pd–PVP (with no O_2 sweep); Pd 8.3 or 83 mg L^{-1}, NaBr 20–400 μN, H_2SO_4 10 or 100 μN, Δ Pd/C (with no O_2 sweep); Pd 8.0 or 79 mg L^{-1}, NaBr 20–400 μN, H_2SO_4 100 μN, ▲ Pd/C (with O_2 sweep, Ref. [5]); Pd 8.0 mg L^{-1}, NaBr 10–100 μN, H_2SO_4 0–1000 μN.

formation proceeded via a L–H mechanism, and the H_2O_2 selectivity (S_f) was greatly affected by the p_{H2}. The hydrogenation of H_2O_2 also followed the L–H mechanism. On Pd/C [5], the rate-determining step was the activation of H_2 for both the H_2–O_2 reaction and the H_2O_2 hydrogenation. The r_0 value was proportional to the p_{H2} and subject to L–H type depression by O_2. S_f was not affected by the p_{H2} or the p_{O2}, and k_d was proportional to the p_{H2} and inversely proportional to the p_{O2}.

Our studies [4, 5], this work] have shown that there are three types of kinetic patterns for the H_2–O_2 reaction on Pd–PVP and Pd/C. The first one is that H_2 activation is rate determining, and H_2O_2 is produced with good selectivity that is independent of the p_{H2} on the Pd/C catalyst in the presence of H^+ and Br^-. Second, the reaction rate is consistent with an L–H mechanism and exhibits high H_2O_2 selectivity that is dependent on the p_{H2} on the Pd–PVP catalyst in the presence of H^+ and Br^-. The last one is that H_2 activation is rate determining, but H_2O_2 is not produced due to the low S_f and the very large k_d on the Pd/C and the Pd–PVP catalysts in the absence of Br^-. It would be reasonable to postulate that these kinetic patterns are closely related to the three classes of Pd sites.

Before discussing the active sites for the H_2–O_2 reaction, the influence of PVP on the catalysis should be discussed, even though no direct evidence of the properties for PVP-covered Pd nano-particles was obtained in this study. The effect of PVP on the catalysis or physicochemical properties of Au nano-particles has been reported [12,13]. However, these studies were performed in the gas phase [12] or under strong adsorption of PVP [13] where no desorption of PVP was allowed. In the present experiment, no or very weak adsorption of PVP on the Pd surface could be the basis of the following observations. The adsorption of Br^- was not retarded in the presence of PVP, as shown in Fig. 8. In a separated experiment, it was confirmed that PVP was added to the reaction system of Pd/C but yielded no kinetic affect on the H_2–O_2 reaction. The observed kinetics in the absence of Br^- was similar on both catalysts, which might support the proposal.

3.3.2. Surface states active for the reaction

The kinetic differences could be attributed to the divergence of the Pd surface structure. In the previous study, two kinds of sites, Sites A and B, were proposed where Site A is coordinatively more unsaturated (e.g., a corner and an edge) and Site B is more saturated (e.g., a plane) [5]. The types of the sites were re-categorized here in more detail. The corner Pd atoms are the most unsaturated and were claimed to adsorb HBr strongly even in the presence of H_2 [5]. Fig. 8 suggested that there was a large amount of highly unsaturated sites on the Pd–PVP nano-colloid catalyst. The following three types of sites have been proposed: the most coordinatively unsaturated sites, such as a corner (Site A_1); moderately unsaturated sites, such as an edge (Site A_2); and the least unsaturated sites, such as (111) surface (Site B). There might be other types of sites, such as (100) and (110) surfaces and various defects, and these sites would be classified as one of the three types depending on their properties.

Site B might occupy a major portion of the surface of the Pd/C catalyst and would be the most effective for the production of H_2O_2 from H_2 and O_2 [5]. Theoretical calculations of the H_2O_2 synthesis on Pd(111) was reported, but Pd(111) was not determined to be the best catalyst [14]. Zhou et al. claimed that the (110) face was the most effective among the (111), (110), and (100) faces [15].

Site A_2 played a major role in the catalysis on Pd–PVP in the presence of H^+ and Br^- and would catalyze the H_2–O_2 reaction via an L–H mechanism. HBr would adsorb on the site but not block all of the sites in the presence of H_2 and O_2. The influence of the p_{H2} on the H_2O_2 selectivity is characteristic of the Pd–PVP catalyst (Fig. 2). O–O cleavage of the $M(O_2)$ species to form 2MO or of the M–OOH species to form MO and MOH would become favorable at low p_{H2}. Both of these reactions have been proposed as the routes for the formation of water. DFT calculations showed that the energy barrier of $M(O_2)$ and M–OOH cleavages was 13.6 and 8.1 kcal mol^{-1} on Pd(111) [14], which indicated that these reactions are facile. In addition, the dissociative chemisorption of O_2 was suggested to lead to the formation of water on more energetic sites, such as defects, edges, and corners [16].

Site A_1 would be responsible for the non-selective H_2–O_2 reaction in the absence of Br^-. The H_2O_2 decomposition activity of Pd/C in the absence of Br^- was very high, and a very small amount of Br^- in addition to the H^+ drastically depressed the H_2O_2 decomposition [5], which indicated the high activity of Site A_1. Although the mechanism is unknown, a corner atom has more vacant coordination positions than an edge atom and might be active not only for the H_2O_2 decomposition but also for the H_2–O_2 reaction.

Finally, the surface state of Pd–PVP will be discussed briefly. The Br^- adsorption measurement (Fig. 8) suggested that there were many highly unsaturated sites, such as A_1 on Pd–PVP. There are a few reports concerning the complication of nano-particle surfaces with certain treatments. The shape of a Pt nano-particle supported on CeO_2 was converted from a particle with (111) and (200) facets to a multi-facet particle under CO and O_2 atmosphere [17]. The PVP-protected metal nano-particles grew or coagulated upon chemical reduction [18]. These reports would support the present speculation that the surface of the Pd–PVP catalyst is occupied by multi-facets, has many corner sites, and is highly reactive.

4. Conclusions

Kinetics of the direct synthesis of H_2O_2 and the related reactions on the Pd–PVP colloid catalyst were found to be distinctly different from that of the Pd/C catalyst. Based on the kinetics and the Br^- adsorption measurement, the following conclusions were found. Surface sites on Pd particles could be categorized into 3 classes according to the degree of coordinative unsaturation. Site A_1 is the most unsaturated site and includes corner sites. Site A_2 is moderately unsaturated and involves edge sites. Site B is the least unsaturated site (i.e., plane). The Pd–PVP contains more A_1 and A_2 sites than the Pd/C. Site A_1 is blocked in the presence of H^+ and Br^- but is the main reaction site in the absence of Br^- producing only H_2O. The major reaction sites on the Pd–PVP in the presence of H^+ and Br^- would be Site A_2, and the adsorbed species, such as PdH_2, $Pd(O_2)$, and H–Pd–OOH, would be more stable on this site than on Site B. The H_2O_2 synthesis and hydrogenation reactions proceeded via the L–H mechanism. The amount of Site B was small on Pd–PVP, and its role for the H_2O_2 synthesis would be limited. In contrast, Site B was the primary site on Pd/C, and the H_2O_2 synthesis would proceed on this site. The large difference in the site distributions between Pd–PVP and Pd/C would explain the difference in the observed kinetics.

Acknowledgments

The authors thank Tanaka Kikinzoku Kogyo K.K. for supplying the Pd–PVP colloid catalyst and providing helpful discussion. This work was financially supported by three Grants-in-Aids (JSPS, NEDO, and ALCA) from the Ministries, MEXT, and METI of Japan.

Appendix A. Supplementary material

Supplementary data associated with this article can be found, in the online version, at doi:10.1016/j.jcat.2011.12.004.

References

[1] J.H. Lunsford, J. Catal. 216 (2003) 455.
[2] J.K. Edwards, G.J. Hutchings, Angew. Chem. Int. Ed. 47 (2008) 9192.
[3] C. Samanta, Appl. Catal. A: Gen. 350 (2008) 133.
[4] T. Deguchi, M. Iwamoto, Ind. Eng. Chem. Res. 50 (2011) 4351.
[5] T. Deguchi, M. Iwamoto, J. Catal. 280 (2011) 239.
[6] Q. Liu, J.C. Bauer, R.E. Schaak, J.H. Lunsford, Angew. Chem. Int. Ed. 47 (2008) 6221.
[7] Y. Nomura, T. Ishihara, Y. Hata, K. Kitawaki, K. Kaneko, H. Matsumoto, ChemSusChem 1 (2008) 619.
[8] D. Dissanayake, J.H. Lunsford, J. Catal. 206 (2002) 173.
[9] D.P. Dissanayake, J.H. Lunsford, J. Catal. 214 (2003) 113.
[10] S. Chinta, J.H. Lunsford, J. Catal. 225 (2004) 249.
[11] Y. Voloshin, R. Halder, A. Lawal, Catal. Today 125 (2007) 40.
[12] H. Tsunoyama, N. Ichikuni, H. Sakurai, T. Tsukuda, J. Am. Chem. Soc. 131 (2009) 7086.
[13] M. Okumura, Y. Kitagawa, T. Kawakami, M. Haruta, Chem. Phys. Lett. 459 (2008) 133.
[14] R. Todorovic, R.J. Meyer, Catal. Today 160 (2011) 242.
[15] B. Zhou, L.-K. Lee, Hydrocarbon Technologies, US 6168,775.
[16] S. Abate, G. Centi, S. Melada, S. Perathoner, F. Pinna, G. Strukul, Catal. Today 104 (2005) 323.
[17] H. Yoshida, K. Matsuura, Y. Kuwauchi, H. Kohno, S. Shimada, M. Haruta, S. Takeda, Appl. Phys. Express 4 (2011) 065001.
[18] N. Toshima, M. Harada, T. Yonezawa, K. Kushibashi, K. Asakura, J. Phys. Chem. 95 (1991) 7448.